Korean J. Chem. Eng., **23**(6), 1028-1033 (2006)

Evaluation of the characteristics using slow strain rate tests of 5456 Al-Mg alloy for ship construction

Seong-Jong Kim†, Jae-Yong Ko and Min-Su Han

Mokpo Maritime University, Chukkyo-dong, Mokpo City, Cheonnam 530-729, Korea
(*Received 2 September 2005 • accepted 18 July 2006*)

Abstract–Recently, there has been increased interest in using aluminum alloys in ship construction instead of fiber-reinforced plastic (FRP). Aluminum alloy ships are faster, have a greater load capacity, and are easier to recycle than FRP ships. We investigated the mechanical and electrochemical properties of aluminum alloys using slow strain rate and potentiostatic tests under various potential conditions. Aluminum and aluminum alloys do not corrode due to the formation of an anti-corrosive passive film, such as Al_2O_3 or $Al_2O_3 \cdot 3H_2O$, which resists corrosion in neutral solutions. In seawater, however, Cl^- ions destroy this passive film. The optimum protection potential range with regards to hydrogen embrittlement and stress corrosion cracking was determined to lie between −1.5 and −0.7 V (SSCE). These results can be used as reference data for ship design.

Key words: Aluminum Alloys, Fiber-Reinforced Plastic (FRP), Electrochemical Property, Hydrogen Embrittlement, Stress Corrosion Cracking

INTRODUCTION

Recently, there has been a new appreciation of aluminum alloys as materials that are capable of reducing the environment load. They are lightweight, easy to recycle, permit miniaturization, and have environmental friendly properties [Tanabe, 2001]. Conversely, fiber-reinforced plastic (FRP) ships, including small fishing boats, have many environmental and recycling problems, and there is no method to decommission an FRP ship. In addition, FRP ships and wooden vessels are small. Medium and large ships cannot detect these FRP and wooden vessels, since the ability of composite materials to reflect radar waves is poor. Therefore, a large proportion of ship accidents involve these vessels. According to data collected by Maritime Affairs and Fisheries in 2002, 72.4% of all marine accidents between 1998 and 2002 and approximately 58% of all collision accidents involved fishing boats [Kim, 2005].

If aluminum were used as a substitute for FRP in ships and boats, the result would be more environmentally friendly vessels that are easy to recycle and have the added value of reduced fuel consumption, higher speed, and increased load capacity. For the last few decades, developed nations, including European nations, Australia, and Japan, have progressively suggested using aluminum alloys for small-vessel construction. In addition, there are ongoing aluminum shipbuilding investigations in Japan with the aim of improving ship construction and welding methods. Aluminum ships have been constructed since 1977; there were 1,670 aluminum vessels by 2001 and the number continues to increase [Sky Al Products Corporation, 2003]. However, only a few aluminum ships have been built in Korea, and the technique is no longer practiced. There are currently only 20 technicians trained in aluminum welding in Korea. Therefore, studies of systematic aluminum welding are very important [Kang, 2004]. According to the Korean Marine Technology Development Plan (July 28, 2004), which aims to develop Korea into a strong maritime nation, the development of marine technology businesses must start in earnest. That development includes aluminum alloy ships [Ministry of Maritime Affairs and Fishers, 2004].

Therefore, this study investigated the mechanical and electrochemical properties of this alloy under various potential conditions using slow strain rate tests. These results will provide reference data for ship design by determining the optimum protection potential with regards to hydrogen embrittlement and stress corrosion cracking.

EXPERIMENTAL

The main additional element of an Al-Mg alloy is magnesium. Al-Mg alloys have high strength and good welding properties. They are often used as materials for vessels and other marine structures since they have good corrosion resistance in a seawater environment. Table 1 shows the mechanical properties and chemical composition of 5456-H116 Al alloy.

The 5456 Al alloy specimens used for electrochemical tests in this investigation were mounted with epoxy resin, leaving an exposed area of 10 mm^2, and then polished with #600 emery paper. The specimens were carefully degreased with acetone and water. The corrosion potential was measured over 24 hours in natural seawater. The polarization system consisted of a Pt coil, which acted as a counter electrode, and an Ag/AgCl saturated KCI reference electrode. The tests were carried out at a scan rate of 2 mV/s at room temperature. The anodic and cathodic polarization took effect from the open circuit potential to +3.0 and −2.0 V (SSCE) for the Ag/AgCl electrode. The test specimens measured 235×4×6 mm (long×wide×thick). Notches, 1 mm wide and deep, were made on both sides of parallel parts of the specimens to cause a fracture. A schematic diagram of a specimen is shown in Fig. 1.

The specimens used for the slow strain rate tests (SSRTs) were also exposed to natural seawater. These were fitted with a jig for an

†To whom correspondence should be addressed.
E-mail: ksj@mmu.ac.kr

Table 1. Mechanical properties and chemical composition of 5456-H116

Mechanical properties	Tensile strength (MPa)			Yield strength (MPa)			Elongation (%)		
	534.1			397.9			14		
Chemical composition	Si	Fe	Cu	Mn	Mg	Cr	Zn	Ti	Al
	0.08	0.20	0.05	0.79	4.80	0.09	0.09	0.02	Balance

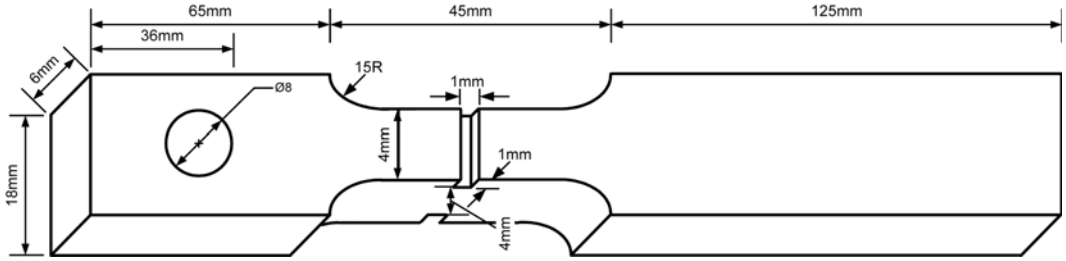

Fig. 1. Schematic diagram of specimen for slow strain rate test.

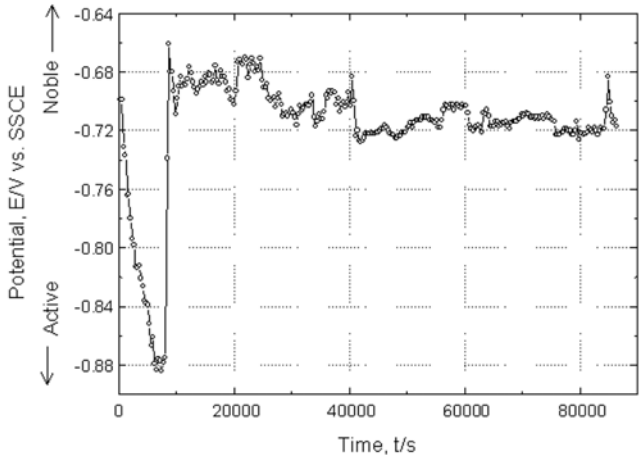

Fig. 2. Variation of potential for 5456 specimen during 86400 s in natural sea water solution.

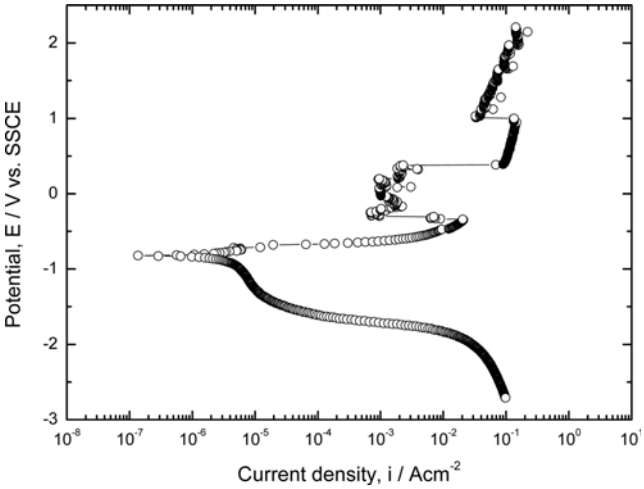

Fig. 3. Anodic and cathodic polarization curve for 5456 Al alloy in natural sea water solution.

Instron machine. The SSRTs was carried out at a strain rate of 0.001 mm/min, during which a constant potential was maintained with a potentiostat/galvanostat apparatus.

RESULTS AND DISCUSSION

Fig. 2 shows the variation in the potential for a 5456 Al alloy specimen during a 24-hour exposure in natural seawater. In general, aluminum and aluminum alloys do not corrode due to the formation of anti-corrosive films, such as Al_2O_3 and $Al_2O_3 \cdot 3H_2O$, in neutral solutions. In the early stages of immersion, however, the corrosion potential of the aluminum alloy shifted abruptly in the more active direction with the destruction of the film caused by the Cl^- ions in the seawater. The potential at 8,000 s was −0.88 V; this increased abruptly to −0.68 V at 10,000 s as a protective film was formed. Thereafter, the potential remained steady until 40,000 s, when it shifted in the active direction with destruction of the film by the Cl^- ions. Stable potential values were obtained for the rest of the test.

Anodic and cathodic polarization curves for 5456 Al alloy in natural seawater are shown in Fig. 3. The anodic polarization was observed as a sudden increase in the current density from the open circuit potential. Thereafter, the current density at a potential of −0.4 V decreased. This phenomenon was likely caused by the formation of a passive film in the seawater. The passivity was maintained at +0.4 V. Then, the current density increased with the destruction of the passive film. Passivity reoccurred due to the self-healing property of aluminum. The cathodic polarization showed concentrated polarization caused by the dissolved oxygen reduction reaction and activation polarization caused by hydrogen generation. The current density in the passivity range of the anodic polarization curve was greater than that in the dissolved oxygen reduction reaction range of the cathodic polarization curve. This suggests that cathodic protection is beneficial compared to anodic protection from an economic viewpoint. However, a previous study revealed that anodic protection at the passivity potential for friction stir welding of 1050 Al specimens was more beneficial compared to cathodic protection from an economic viewpoint [Jang, 2004]. In addition, the corrosion improvement effects obtained in aluminum with friction stir

welding are accompanied by relief of the residual stresses due to the frictional heat.

For the cathodic polarization of 5456 Al alloy, the turning point between concentration polarization due to the oxygen reduction reaction ($O_2+2H_2O+4e \rightarrow 4OH^-$) and activation polarization due to hydrogen gas generation ($2H_2O+2e \rightarrow H_2+2OH^-$) was approximately −1.70 V (SSCE) in our tests. In the anodic polarization curve, passivity reoccurred due to the self-healing property of aluminum, indicating that the passive film was restored. However, a large-scale increase in the current density in the cathodic polarization curve was observed at the potential generated by hydrogen gas. In addition, corrosion similar to hydrogen generation occurred at the potential of both the acidic and alkaline solutions, according to the E-pH diagram of aluminum [Pourbaix, 1974].

An aluminum E-pH diagram was derived from the protection range, since the pH of seawater is approximately 8.0. However, the passivity phenomenon did not occur due to destruction of the passivity film caused by the Cl^- ions. The characteristics of aluminum in seawater differed from those of aluminum in other neutral solutions.

Fig. 4 shows the current density of the 5456 Al alloy in natural seawater after the 1,200-s long potentiostatic tests. The potential ranged from −0.68 to −1.5 V, which indicates a low current density. This low current density gives an estimate of the protection potential range. The current density increased suddenly when the potential shifted beyond the potential protection range in either the anodic or cathodic directions. This trend was observed from the polarization curves. However, the critical potentials that mark the onset of hydrogen embrittlement, and stress corrosion cracking cannot be determined from the polarization curves alone. Therefore, SSRTs were also carried out as functions of the anodic and cathodic potentials to investigate the mechanical and electrochemical properties of the specimens.

The stress-elongation curves obtained when SSRTs were performed on specimens in seawater at 0 (no protection), −0.5, −0.65, and −0.7 V are shown in Fig. 5. The elongation at 0 V was high. However, corrosion protection under these conditions was impossible because the toughness of the material was low due to the decreased strength resulting from the active dissolution reaction in parallel parts of the specimen. The tests confirmed that the strength and elongation in seawater with no protection were greater than those obtained at −0.5 and −0.65 V. These potentials were the result of a dissolution reaction while the current density increased from the open circuit potential. Conversely, the measured strength and elongation were greater than those obtained in seawater when the applied potential was −0.7 V. This suggests that the protection potential condition was reached. In addition, the current density given by the polarization curve at a potential of −0.7 V was less than that obtained at potentials of −0.5 and −0.65 V.

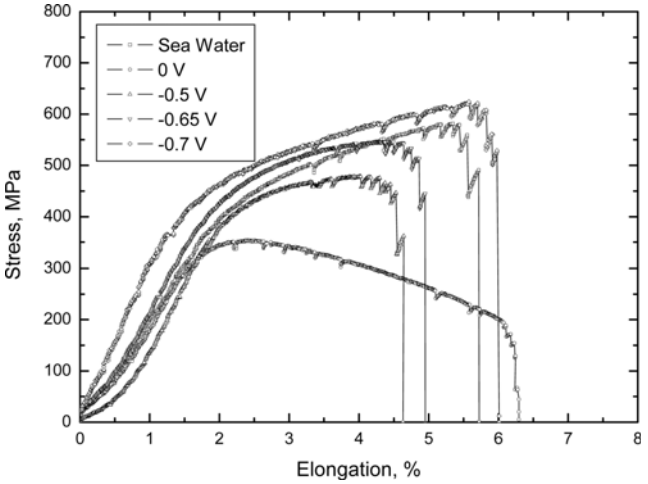

Fig. 5. Stress-elongation curves in sea water and the applied potential of 0 V, −0.5 V, −0.65 V and −0.7 V during slow strain rate test in natural sea water solution.

Fig. 6 shows the stress-elongation curves at −0.8, −0.9, −1.1, and −1.3 V obtained during the SSRTs for specimens in natural seawater. In the SSRTs, the current densities at potentials ranging between −1.3 and −0.8 V were low in the cathodic polarization curve. This low current density indicates the range of concentration polarization due to the dissolved oxygen reduction reaction. The best mechani-

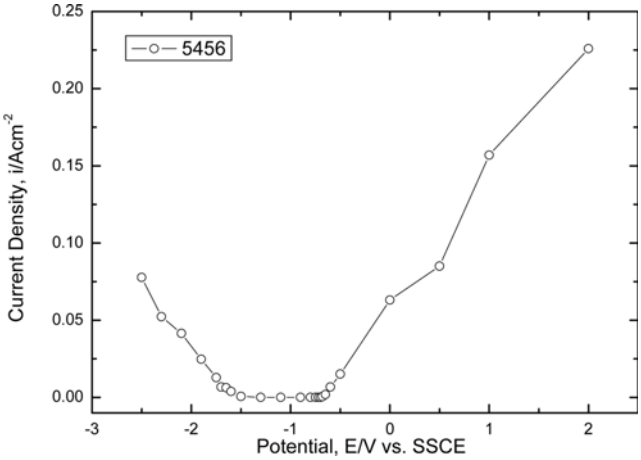

Fig. 4. Comparison of current density after potentiostatic experiment during 1,200 sec for 5456 Al alloy in natural sea water solution.

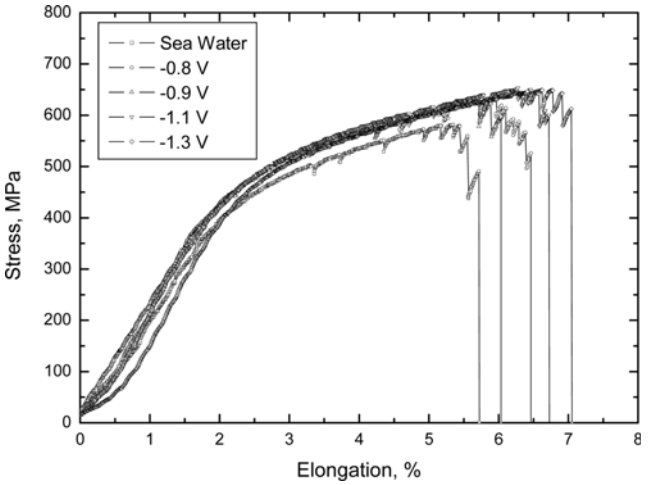

Fig. 6. Stress-elongation curves in sea water and the applied potential of −0.8 V, −0.9 V, −1.1 V and −1.3 V during slow strain rate test in natural sea water solution.

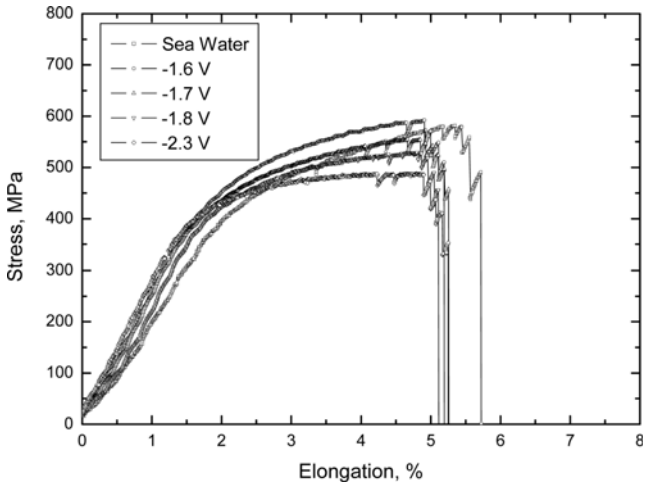

Fig. 7. Stress-elongation curves in sea water and the applied potential of –1.6 V, –1.7 V, –1.8 V and –2.3 V during slow strain rate test in natural sea water solution.

cal properties were obtained at –1.3 V. The mechanical properties at potentials between –1.3 and –0.8 V were better than those for seawater with no protection. This suggests that potentials between –1.3 and –0.8 V are suitable for cathodic protection.

The stress-elongation curves obtained from the SSRTs in natural seawater at –1.6, –1.7, –1.8, and –2.3 V are shown in Fig. 7. As shown in the polarization curve, the potential range of –1.6 to –1.8 V corresponded to the turning point between concentration polarization due to the oxygen reduction reaction ($O_2+2H_2O+4e \rightarrow 4OH^-$) and activation polarization due to hydrogen generation ($2H_2O+2e \rightarrow H_2+2OH$). The elongation measured at potentials between –1.6 and –2.3 V was less than that obtained in seawater. Therefore, this range consists of over-protection potentials. These potentials are close to the corrosion protection range in the cathodic polarization curves. However, the embrittlement phenomenon also occurred due to atomic hydrogen at the lower potentials and molecular hydrogen at –2.3 V. This caused the lowest maximum tensile strength and elongation values to occur at –2.3 V. The maximum tensile strength and elongation decreased when the potential shifted in the low cathodic potential direction. Moreover, from investigations of hydrogen embrittlement in high-strength steel [Kim et al., 2002, 2003], the turning point between concentration polarization due to the oxygen reduction reaction and activation polarization due to hydrogen gas generation is approximately –1,000 mV (SCE). A potential of –900 mV (SCE) was also included in the range of concentration polarizations examined in this study due to the dissolved oxygen reduction reaction. The appearance of hydrogen embrittlement at –900 mV (SCE) was caused by atomic hydrogen.

Fig. 8 compares effects of the applied potential on the maximum tensile strength when the SSRTs were performed on specimens in natural seawater. The maximum tensile strength for applied potentials between –1.6 and –0.7 V was greater than that obtained in seawater, 581.71 MPa. The potential range that yielded a low current density in the potentiostatic tests in Fig. 4 (–1.5 to –0.68 V) is similar to this applied potential range (–1.6 to –0.7 V). Therefore, the protection potential range lies between –1.6 and –0.7 V. The maximum tensile strength decreased when the potential shifted beyond this range in either the anodic or cathodic directions. When the potential shifted in the anodic direction, the tensile strength decreased due to an active dissolution reaction. In particular, 0 V gave the lowest value of 353.38 MPa.

Fig. 9 presents the effects of the applied potential on the yield strength when the SSRTs were performed on specimens in natural seawater. There was no correlation between the yield strength and applied potential. The highest yield strength was obtained at an applied potential of –1.3 V. Conversely, the lowest yield strength appeared for 0 V.

Previous investigations of hydrogen embrittlement in high-strength steel exposed to a seawater environment were not able to find correlations between the tensile strength, yield strength, and applied cathodic potential, regardless of the welding method or post-welding heat treatment [Kim et al., 2002, 2003]. However, we identified a correlation between the maximum tensile strength and applied potential in the Al alloy, indicating different trends between the two materials.

The effects of the applied potential on elongation when the SSRTs

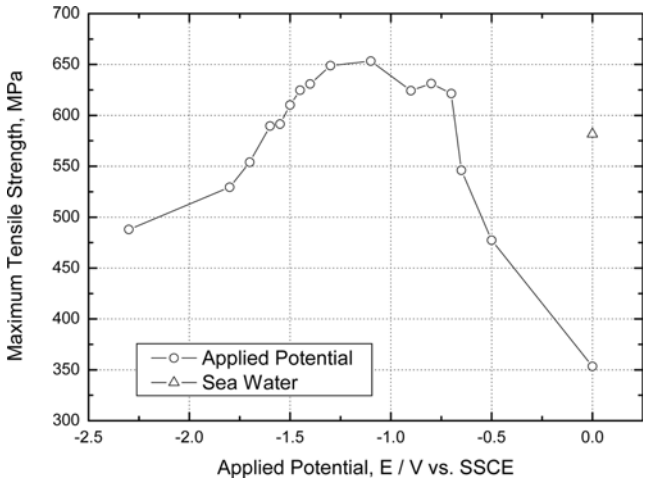

Fig. 8. Effects of applied potential for maximum tensile strength after SSRT in natural sea water.

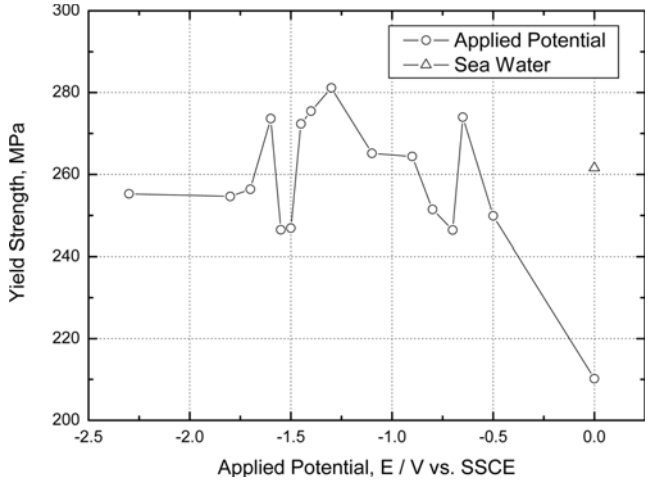

Fig. 9. Effects of applied potential for yield strength after SSRT in natural sea water.

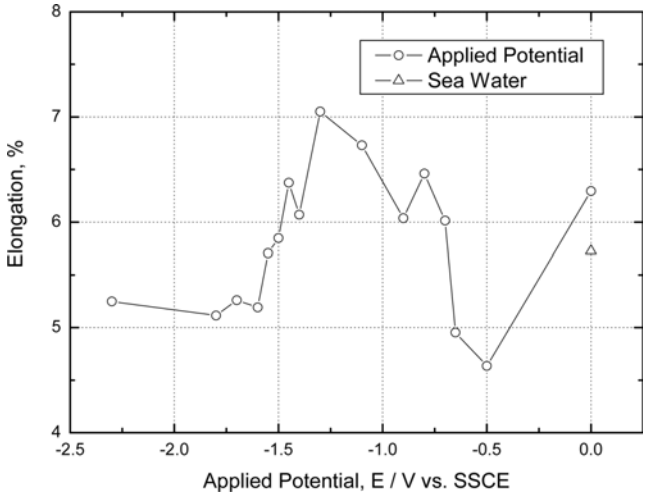

Fig. 10. Effects of applied potential for elongation after SSRT in natural sea water.

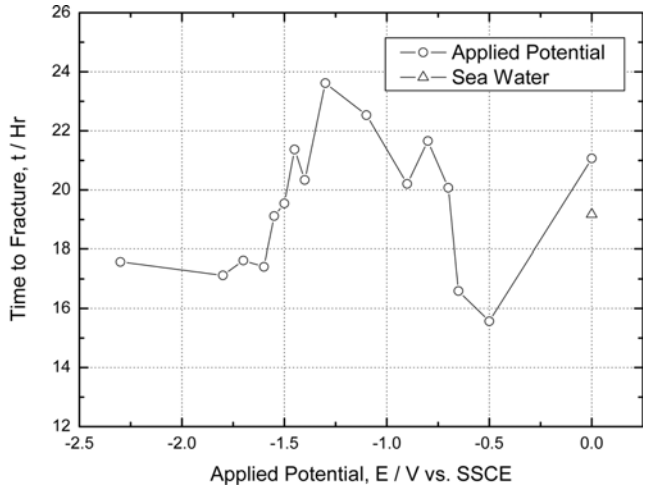

Fig. 11. Effects of applied potential for time-to-fracture after SSRT in natural sea water.

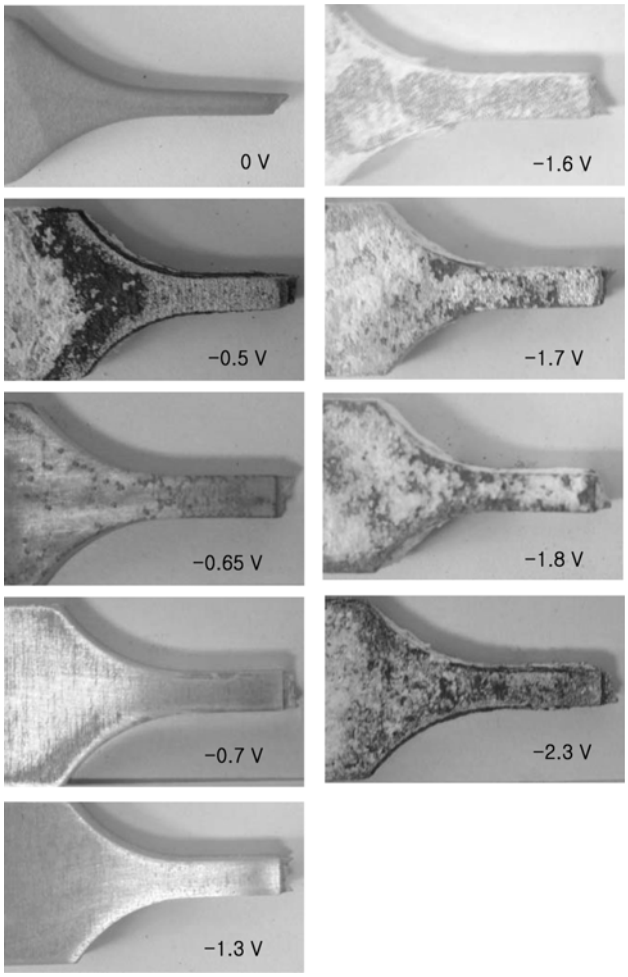

Fig. 12. Photographs of fractured specimen after SSRT at various applied potential in natural sea water solution.

were performed on specimens in natural seawater are shown in Fig. 10. The elongation at applied potentials ranging between −1.5 and −0.7 V was greater than for seawater conditions, similar to the maximum tensile strength. In particular, the greatest elongation was obtained for 0 V. Additional protection was impossible since the tensile strength was very low. The elongation decreased when the potential shifted beyond this range in either the anodic or cathodic directions. Therefore, −1.5 to −0.7 V corresponds to the protection potential range.

Fig. 11 shows the effects of the applied potential on the time-to-fracture when the SSRTs were performed on specimens in natural seawater. The time-to-fracture for potentials ranging from −1.5 to −0.7 V was greater than that obtained for seawater conditions, similar to the maximum tensile strength and elongation. The elongation and time-to-fracture at an applied potential of 0 V were high. However, corrosion protection was impossible at 0 V because the material toughness was low due to the decreased strength resulting from the active dissolution reaction. The time-to-fracture decreased when the potential shifted to more anodic or cathodic values outside the range −1.5 to −0.7 V.

Low current densities, *i.e.*, the protection potential obtained from the potentiostatic experiment after 1,200 s, appeared between −1.5 and −0.68 V. This includes the potential range that exhibited good mechanical properties as determined by the SSRTs.

Fig. 12 shows photographs of fractured specimens after the SSRTs were performed at various applied potentials in natural seawater. The lowest maximum tensile strength and yield strength were obtained for an applied potential of 0 V due to the active dissolution reaction in parallel parts of the specimens. Corroded features due to pitting were observed for applied potentials of −0.5 and −0.65 V. The dissolution phenomenon was more evident at −0.5 V compared to −0.65 V because of the high current density in the anodic polarization curve. In addition, the fractured specimens obtained for −1.3 to −0.7 V were very clean due to perfect protection, while those obtained for −2.3 to −1.6 V had a white coating consisting of a calcareous deposit composed of $Mg(OH)_2$ and $CaCO_3$, which was formed at the cathode surface due to the cathodic protection in seawater [Deslouis et al., 1998, 2000; Neville et al., 2002; Simpson, 1998; Barchiche et al., 2003]. The calcareous deposit was generated from the following reactions:

$O_2+2H_2O+4e^- \leftrightarrow 4OH^-$ (dissolved oxygen reduction reaction) (1)

$2H_2O+2e^- \leftrightarrow 2OH^-+H_2$ (hydrogen generation reaction) (2)

Moreover, CO_2 emitted in the air is dissolved in seawater according and combines with H_2O as given by

$$CO_2+H_2O \rightarrow H_2CO_3 \quad (3)$$

H_2CO_3 dissociates readily, as given by

$$H_2CO_3 \rightarrow H^+ + HCO_3^- \quad (4)$$

$$HCO_3^- \rightarrow H^+ + CO_3^{2-} \quad (5)$$

since the combination force of H_2CO_3 formed by equation (3) is weak compared to the combination force of H_2O. Therefore, CO_3^{2-} forms on the cathodic polarized metal surface, in addition to OH^-. The CO_3^{2-} and OH^- ions combine with Ca^{2+} or Mg^{2+} ions as given by

$$CO_3^{2-}+Ca^{2+} \rightarrow CaCO_3 \quad (6)$$

$$2OH^-+Mg^{2+} \rightarrow Mg(OH)_2 \quad (7)$$

Consequently, a calcareous deposit composed of $CaCO_3$ and $Mg(OH)_2$ forms at the cathode surface.

The film composed of $CaCO_3$ and $Mg(OH)_2$ provides corrosion resistance. However, a uniform electrodeposition coating does not form at potentials below –1.6 V due to the lack of time. Therefore, we concluded that the mechanical properties at such potentials were poor because the effect of hydrogen gas generation exceeded that of electrodeposition.

From the results presented here, the optimum protection potential range obtained by considering the potentiostatic tests, maximum tensile strength, elongation, and time to fracture lies between –1.5 and –0.7 V (SSCE).

CONCLUSIONS

Slow strain rate tests were used to evaluate the characteristics of high-strength Al-Mg alloy (5456) for application in ships. The following conclusions were drawn from this study. Aluminum and aluminum alloys do not corrode due to the formation of an anticorrosive passive film, such as Al_2O_3 or $Al_2O_3 \cdot 3H_2O$, which resists corrosion in neutral solutions. In seawater, however, Cl^- ions destroy this passive film. In the potentiostatic tests, the current density in the potential range from –0.68 to –1.5 V after 1,200 s was low. This low current density indicated the protection potential range. Elongation at an applied potential of 0 V was high. However, corrosion protection under these conditions was impossible because the toughness of the material was low due to the decreased strength resulting from the active dissolution reaction in parallel parts of the specimen. A film composed of $CaCO_3$ and $Mg(OH)_2$ provides corrosion resistance. However, a uniform electrodeposition coating did not form at potentials below –1.6 V due to a lack of time. Therefore, we concluded that the mechanical properties at such potentials were poor because the effect of hydrogen gas generation exceeded that of electrodeposition. After considering the results of the potentiostatic tests, maximum tensile strength, elongation, and time-to-fracture, we conclude that the optimum protection potential range was between –1.5 and –0.7 V (SSCE).

REFERENCES

Barchiche, Ch., Deslouis, C., Festy, D., Gil, O., Refait, P., Touzain, S. and Tribollet, B., "Characterization of calcareous deposits in artificial sea water by impedance techniques-3. Deposit of $CaCO_3$ in the presence of Mg(II)," *Electrochimica Acta*, **48**, 1645 (2003).

Deslouis, C., Festy, D., Gil, O., Maillot, V., Touzain, S. and Tribollet, B., "Characterization of calcareous deposits in artificial sea water by impedance techniques-2. Deposit of $Mg(OH)_2$ without $CaCO_3$," *Electrochimica Acta*, **45**, 1837 (2000).

Deslouis, C., Festy, D., Gil, O., Rius, G, Touzain, S. and Tribollet, B., "Characterization of calcareous deposits in artificial sea water by impedance techniques-1. Deposit of $CaCO_3$ without $Mg(OH)_2$," *Electrochimica Acta*, **43**(12-13), 1891 (1998).

Jang, S. K., Lee, D. C., Kim, S. J., Jeon, J. I. and Kim, S. H., "Investigation of macrostructures and properties for friction stir welded 1050 aluminum alloy sheet," *The Proceedings of Korean Society of Marine Engineers*, 139 (2004).

Kang, B. Y. and Cho, J. H., "Consideration for structure and fabrication procedure of Al boat," *The Korean Journal of Welding Society*, **22**(3), 39 (2004).

Kim, S. J. and Moon, K. M., "Hydrogen embrittlement properties of heat affected zone of high strength steel in shielded metal arc welding," *Metals and Materials International*, **8**(4), 395 (2002).

Kim, S. J. and Moon, K. M., "The relationship between corrosion protection and hydrogen embrittlement properties of HAZ in flux cored arc welding," *Metals and Materials International*, **8**(4), 387 (2002).

Kim, S. J., Ko, J. Y., Jang, S. K. and Kim, J. I., "Evaluation of mechanical and electrochemical properties of materials for Al ship in sea water environment," *Proceedings of the Korean Society of Marine Environment and Safety*, 161 (2005).

Kim, S. J., Okido, M. and Moon, K. M., "An electrochemical study of cathodic protection of steel used for marine structures," *Korean J. Chem. Eng.*, **20**, 560 (2003).

Kim, S. J., Okido, M. and Moon, K. M., "The electrochemical study on mechanical and hydrogen embrittlement properties of HAZ part as a function of post-weld heat treatment in SMAW," *Surface and coatings Technology*, **169-170**, 163 (2003).

Ministry of Maritime Affairs and Fishers, *Comprehensive Program for Fisheries and the Fishing Industry*, 20 (2004).

Neville, A. and Morizot, A. P., "Calcareous scales formed by cathodic protection-an assessment of characteristics and kinetics," *Journal of Crystal Growth*, **243**, 4890 (2002).

Pourbaix, M., "Atlas of electrochemical equilibria," *NACE*, 168 (1974).

Simpson, L. J., "Electrochemicall generated $CaCO_3$ deposits on iron studied with FTIR and Raman spectroscopy," *Electrochimica Acta*, **43** (16-17), 2543 (1998).

Sky Al products corporation, "Foundation of Al alloy ship projects," *Journal of Japan Institute of Light Metals Welding*, **41**(11), 544 (2003).

Tanabe, Z. and Matsumoto, F., "Actualities and problems of Al alloy for the environmental resistance," *Journal of Japan Institute of Light Metals*, **39**(3), 125 (2001).